

RESEARCH ARTICLE | MARCH 07 2024

## Electromagnetic emission from plasma with counter-streaming electron beams in the regime of oblique instability dominance

V. V. Annenkov (В.В. Анненков)   ; E. P. Volchok (Е.П. Волчок)  ; I. V. Timofeev (И.В. Тимофеев) 



*Phys. Plasmas* 31, 033104 (2024)

<https://doi.org/10.1063/5.0190331>



# Electromagnetic emission from plasma with counter-streaming electron beams in the regime of oblique instability dominance

Cite as: Phys. Plasmas **31**, 033104 (2024); doi: 10.1063/5.0190331

Submitted: 5 December 2023 · Accepted: 14 February 2024 ·

Published Online: 7 March 2024



View Online



Export Citation



CrossMark

V. V. Annenkov (В.В. Анненков),<sup>1,2,a)</sup> E. P. Volchok (Е.П. Волчок),<sup>1</sup> and I. V. Timofeev (И.В. Тимофеев)<sup>1</sup>

## AFFILIATIONS

<sup>1</sup>Budker Institute of Nuclear Physics SB RAS, 630090 Novosibirsk, Russia

<sup>2</sup>Institute of Solar-Terrestrial Physics SB RAS, 664033 Irkutsk, Russia

<sup>a)</sup> Author to whom correspondence should be addressed: [annenkov.phys@gmail.com](mailto:annenkov.phys@gmail.com)

## ABSTRACT

In this study, we investigate the generation of electromagnetic emission near the second harmonic of the plasma frequency induced by pairs of counter-propagating electron beams. Such systems can naturally occur in cosmic plasmas when particle acceleration regions are closely spaced, and they can also be implemented in a laboratory device. We specifically focus on the regime where the oblique beam-plasma instability dominates. The emission mechanism relies on the coalescence of counter-propagating plasma waves with different transverse structures. It has been demonstrated that the parameters of the system necessary for efficient radiation generation can be determined using the exact linear theory of beam-plasma instability. Through particle-in-cell numerical simulations, we show that a high beam-to-radiation conversion efficiency can be achieved when the beams excite small-scale oblique plasma oscillations. Importantly, we find that the efficiency and spectral characteristics of the radiation are not dependent on the thickness of the beams. We explore two scenarios involving pairs of symmetric beams: one with relativistic beams having a directed velocity of  $v_b = 0.9c$  and another with sub-relativistic beams at  $v_b = 0.7c$ . Additionally, we consider the injection of two beams with different velocities. In all cases considered, the beam-to-radiation power conversion efficiency reaches a level of a few percent, a sufficiently high value for beam-plasma systems.

© 2024 Author(s). All article content, except where otherwise noted, is licensed under a Creative Commons Attribution-NonCommercial 4.0 International (CC BY-NC) license (<https://creativecommons.org/licenses/by-nc/4.0/>). <https://doi.org/10.1063/5.0190331>

## I. INTRODUCTION

One of the fundamental problems of plasma physics is the interaction of plasma with fluxes of charged particles, in particular electron beams. Passing through plasma, electron beams cause the development of the two-stream (bump-on-tail) instability,<sup>1,2</sup> which excites plasma oscillations. In open magnetic traps, electron beams have been considered for plasma heating to fusion temperatures and confinement improvement,<sup>3,4</sup> as a promising way to create a target plasma<sup>5</sup> and as a possible source of powerful narrowband electromagnetic emission.<sup>6–8</sup> In tokamaks, certain plasma conditions can lead to the formation of a beam of superthermal electrons (runaway electrons). Understanding of their interaction process with plasma in fusion devices can provide a useful diagnostic instrument and is important in maintaining the stability of the plasma.<sup>9,10</sup> Another field in which the study of the beam-plasma interaction is extremely relevant is astrophysics.<sup>11–15</sup> Accelerated streams of charged particles generated during magnetic reconnection processes<sup>16</sup> or shock wave propagation<sup>17</sup> lead to various physical processes in the solar atmosphere and can also leave it along

open magnetic field lines, reaching Earth's orbit. Typical consequences of the propagation of such beams include plasma heating,<sup>18,19</sup> various processes in natural magnetic traps,<sup>20</sup> and generation of non-thermal radiation.<sup>21,22</sup>

One of the fundamental processes in generating electromagnetic (EM) radiation for interpreting solar radio bursts is the three-wave coupling process of plasma waves  $L$  and  $L'$  into electromagnetic emission near the second harmonic of the plasma frequency  $L + L' \rightarrow T_{2\omega_p}$ .<sup>21</sup> Typically, single-beam systems are considered, where the plasma waves traveling in the opposite direction arise due to nonlinear processes. However, a significant portion of the beam power is lost to plasma heating and excitation of non-radiating harmonics. More complete discussion of possible radiation mechanisms in plasma with a single electron beam can be found in review<sup>22</sup> and textbook.<sup>23</sup> High-efficiency radiation generation in single-beam systems can be achieved, for example, by introducing longitudinal density modulation in the plasma. If the transverse size of the beam-plasma system is an order of plasma wavelength, this modulation will allow the beam-driven modes

to convert their energy to plasma oscillations with superluminal phase velocity, which can resonantly excite vacuum electromagnetic modes at the plasma frequency.<sup>24,25</sup> Coalescence of the primary beam mode with oscillations scattered on density modulation can cause emission near the second harmonic of the plasma frequency.<sup>26</sup> In the case of oblique density modulation, efficient  $\omega_p$  radiation is possible even in thick plasma.<sup>27</sup> The required plasma structures can be self-consistently developed in initially homogeneous plasma under the influence of the modulation instability,<sup>28–30</sup> although this process requires some time and the presence of sufficient conditions for the development.

However, in space plasma, the situation of generation of counter-streaming electron beams can be realized.<sup>31</sup> In the laboratory experiments,<sup>32–34</sup> generation of radiation in such systems was found to be more efficient than in plasmas with a single beam. The possibility to significantly increase the level of EM emission from a plasma with two counter-streaming beams due to the three-wave process under certain conditions has been shown by particle-in-cell (PIC) simulations.<sup>35</sup> However, to realize it, the beam-excited plasma oscillations  $L$  and  $L'$  should be capable to participate in a three-wave process  $L + L' \rightarrow T_{2\omega_p}$ , already during the linear stage of the beam–plasma instability. Thus, the approach has a significant drawback. For efficient emission, a fairly precise localization of the maximum growth rate of beam instability in the  $k$ -space of the three-wave process is required. Such a localization is achieved by fine-tuning of the beam parameters (density, energy, and velocity distribution) as well as background plasma parameters (external magnetic field and temperature). As simulations have shown,<sup>35</sup> even relatively small deviations of system parameters from the found efficient regime lead to a significant decrease in the emission level. Therefore, the first problem lies in the need for fine-tuning the system to achieve the efficient regime, while the second problem is that various natural factors such as inhomogeneity of plasma density or magnetic field can easily take the system out of this regime.

Free from these problems is the plasma emission mechanism based on coalescence of counter-propagating plasma waves with different transverse structures.<sup>36–38</sup> In such a system, scattering of one plasma wave on the density modulation created by another wave produces oscillations of electron current with the superluminal phase velocities and frequency near the second harmonic of plasma one. Such oscillations can resonantly build up EM waves. To achieve high beam-to-radiation conversion efficiency in this process, it is necessary<sup>39,40</sup> that the characteristic scale of inhomogeneity of the transverse structure of each interacting wave should be of the order of  $c/\omega_p$ , where  $c$  is the speed of light in vacuum and  $\omega_p$  is the plasma frequency. One way to excite such waves is to use thin electron beams. In real systems, electron beams usually have significantly larger transverse sizes than the scale of  $c/\omega_p$ . Furthermore, the excitation of purely longitudinal plasma oscillations is not necessarily a characteristic feature. The work<sup>41</sup> demonstrates the fundamental possibility of this mechanism operating in plasma with wide counter-propagating relativistic beams, which excite oblique plasma oscillations. In such a regime, the beam is trapped by the fields of oblique electrostatic modes. As a result, a transverse modulation of the beam density and the amplitude of the beam mode<sup>42</sup> is formed. The result of the nonlinear development of the beam instability is the formation of spatially localized structures with a characteristic scale  $c/\omega_p$ . The same electrostatic fields localized in space can be excited by short drivers having the same transverse size.<sup>39</sup>

The purpose of this paper is to investigate the process of EM emission from thick plasma with counter-streaming electron beams in the regime of oblique plasma mode domination. We will check the possibility of finding emission regimes using exact kinetic linear theory of the beam–plasma instability and to study influence of beam width on emission properties. Since we already know<sup>41</sup> that counter-streaming relativistic beams can efficiently generate emission via this mechanism, other goal is to check such an ability for sub-relativistic beams. Finally, it is more probable that in the real systems beams will have non-equal directed velocities. So, in this work, we will also to investigate the case of different counter-streaming beams. Section II gives basic information about the mechanism of EM emission generation at the second harmonic of plasma frequency due to the interaction of counter plasma oscillations with different transverse structures. In Sec. III, the parameters of the beam–plasma system involved in further particle-in-cell simulations are described. The choice of the parameters is done using an exact kinetic linear theory of the beam–plasma instability, taking into account the influence of an external magnetic field and relativistic effects. Section IV describes the numerical schemes and the computational domain that were used. Section V contains the simulation results. Section VA discusses the injection into plasma of beams with the average velocity  $v_b = 0.9c$ , and Sec. VB—with the average velocity  $v_b = 0.7c$ . In both cases, the injection of a single beam into plasma is initially examined to investigate the convergence in the number of model macro-particles and determine the length at which the beam relaxes. Then, the injection of counter beams is investigated and the dependence of the generated radiation on their transverse size is studied. In Sec. VC, it is shown that the discussed mechanism also works in the case of counter beams with different average speeds and the radiation is generated at an angle to the system axis. In Sec. VI, a discussion of the obtained results and suggestions for their further application are given.

## II. RADIATION MECHANISM

Initially, the mechanism of radiation due to interaction of counter plasma waves was discussed for the case of short laser drivers with small transverse sizes.<sup>39</sup> However, it works well even for wide plasma waves with non-uniform transverse structures.<sup>36,43,44</sup> Detailed description of the underlying theory can be found in the works cited above, while in this section we will limit ourselves to a brief description of its basic essence.

Let us consider counter-propagation of two potential plasma waves ( $\mathbf{E} = -\nabla\Phi$ ) in a cold and unmagnetized plasma

$$\Phi(t, \mathbf{r}) = \Phi_1(\mathbf{r}_\perp) e^{ik_\parallel^{(1)} r_\parallel - i\omega_1 t} + \Phi_2(\mathbf{r}_\perp) e^{-ik_\parallel^{(2)} r_\parallel - i\omega_2 t} + c.c.. \quad (1)$$

Here, waves have a transverse dependence on the coordinate  $\mathbf{r}_\perp$  and propagate freely in the both longitudinal directions  $r_\parallel$ , along the axis of the system, with phase velocities  $v_{ph}^{(1,2)} = \pm\omega_{(1,2)}/k_\parallel^{(1,2)}$ . The scattering of one wave on the density perturbation created by another wave generates a perturbation of plasma electron current

$$\mathcal{J}_\parallel = -(\delta n_1 v_\parallel^{(2)} + \delta n_2 v_\parallel^{(1)}) e^{ik_\parallel^{(rad)} r_\parallel - i\omega_{(rad)} t} + c.c. \quad (2)$$

with the amplitude

$$\mathcal{J}_{amp} = \frac{k_1 k_2}{\omega_1 \omega_2} \left( \frac{k_{\parallel}^{(1)}}{\omega_1} - \frac{k_{\parallel}^{(2)}}{\omega_2} \right) \Phi_1 \Phi_2 + \frac{1}{\omega_1 \omega_2} \left( \frac{k_{\parallel}^{(1)}}{\omega_2} \Phi_1 \Delta_{\perp} \Phi_2 - \frac{k_{\parallel}^{(2)}}{\omega_1} \Phi_2 \Delta_{\perp} \Phi_1 \right) \quad (3)$$

derived from fluid motion and continuity equations.

The frequency of this perturbation will be equal to the sum of the frequencies of the original waves  $\omega_{(rad)} = \omega_1 + \omega_2$ , and the wave number will be equal to the sum of the colliding wave numbers  $k_{\parallel}^{(rad)} = k_{\parallel}^{(1)} + (-k_{\parallel}^{(2)})$ . Such a perturbation can have a superluminal phase velocity  $v_{ph} = \omega_{(rad)}/k_{\parallel}^{(rad)}$  and is therefore able to excite electromagnetic oscillations at the frequency  $\omega_{(rad)}$  in a resonant manner. In the particular case of colliding waves with identical wave vectors, the longitudinal wave number of the resulting perturbation is zero and its phase velocity becomes infinite.

The first term in Eq. (3) depends substantially on the wave numbers of the colliding waves. The wave number  $k$  is determined by the velocity of the drivers. So, first term is smaller the closer to each other velocities of the drivers. Thus, for example, it is exactly zero for waves excited by short laser pulses (traveling at the speed of light), as well as for plasma waves from identical counter-streaming electron beams. The second term can contribute to the radiative current if the transverse profiles of the colliding oscillations are different  $[\Delta_{\perp} \Phi_1(\mathbf{r}_{\perp}) \neq \Delta_{\perp} \Phi_2(\mathbf{r}_{\perp})]$ . According to the theory,<sup>39</sup> the most efficient emission is expected when the cross size of the colliding plasma waves is of the order of  $c/\omega_p$ .

Let us demonstrate this effect using synthetic calculations of propagation in cold unmagnetized plasma of counter plasma waves generated by the ponderomotive force of short laser pulses. For simplicity, we turn off the effect of laser diffraction and ion dynamics. Figure 1 shows the case of plasma waves with the same transverse structure. One can see the absence of radiation before the collision of the pulses, which is an obvious consequence of the potential nature of the plasma waves. After the overlap of the waves with the same shapes, a slight radiation is observed, which quickly ceases. In the case of plasma waves with different transverse structures (Fig. 2), one can see much more powerful emission at the second harmonic of the plasma frequency in the strictly transverse direction. More details on these calculations can be found in the video in the supplementary material.

The plasma is transparent for the second harmonic radiation, and in vacuum, we can use for the EM waves the dispersion relation:  $\omega_{(rad)}^2 = k^2 c^2$ , where  $k^2 = k_{\parallel}^{(rad)2} + k_{\perp}^{(rad)2}$  and  $\omega_{(rad)}$  is the frequency of radiation. In the case of different wavenumbers  $k_{\parallel}^{(1)}$  and  $k_{\parallel}^{(2)}$  of colliding waves, the radiation will have a longitudinal wavenumber  $k_{\parallel}^{(rad)} = k_{\parallel}^{(1)} - k_{\parallel}^{(2)}$  and therefore will exit at some angle. The longitudinal wavenumber and frequency of the generated radiation is determined by the parameters of the colliding waves, so it is not difficult to calculate the resulting transverse wavenumber and angle of emission

$$\alpha = \arctan \left[ \frac{k_{\perp}^{(rad)}}{k_{\parallel}^{(rad)}} \right], \quad (4)$$

where  $k_{\perp}^{(rad)} c = \sqrt{\omega_{(rad)}^2 - k_{\parallel}^{(rad)2} c^2}$ .

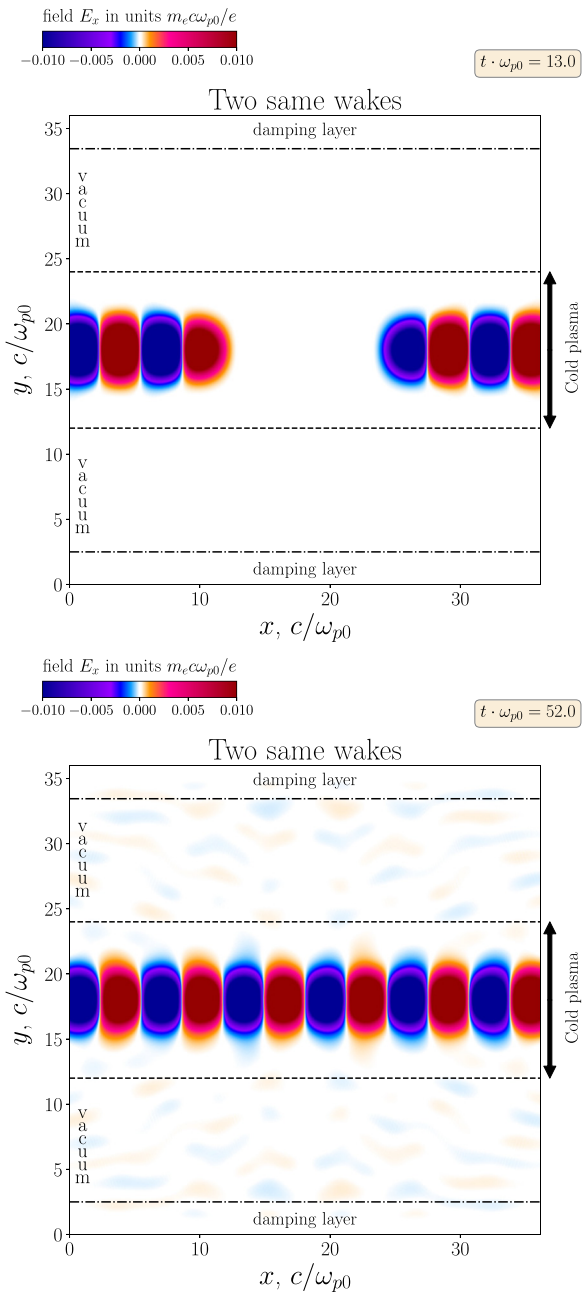
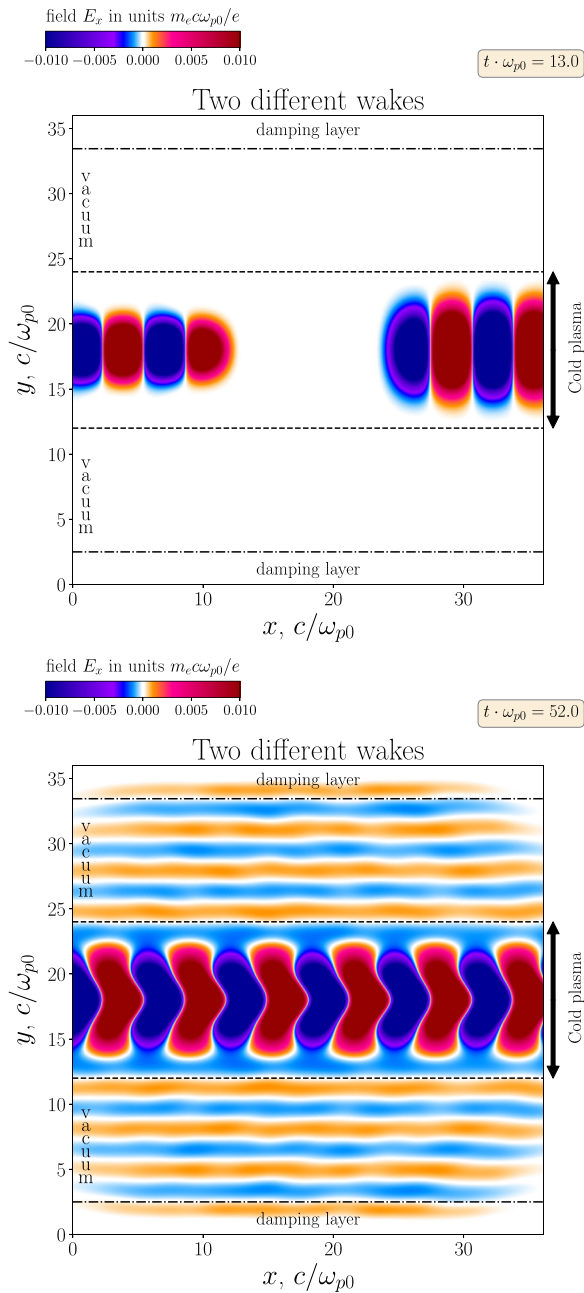


FIG. 1. Counter plasma waves with the same transverse shape.

The angular distribution of such radiation at head-on collision of waves with same wavenumbers coincides with the distribution of a dipole antenna. If there is a small angle between the axes of the drivers, the maximum of intensity appears in the transverse direction to the axis of the narrower pulse.<sup>40</sup>

### III. BEAMS AND PLASMA PARAMETERS

In this work, we consider collisionless fully ionized plasma, which can be created in laboratory devices or take place in solar atmosphere.



**FIG. 2.** Counter plasma waves with the different transverse shapes.

First of all, it is necessary to choose those parameters of the beam–plasma system at which oblique oscillations with a transverse wavelength of the order of units  $c/\omega_p$  are the most unstable. Dominance of such oscillations in the unstable spectrum is primarily a result of relativistic speed of the beam particles. In this case, due to relativistic mass anisotropy, the oscillations transverse to the beam propagation direction appear to be easier to excite.<sup>45,46</sup> From the linear theory, it is possible to estimate which oscillations will be excited. In

the case of relativistic beams in a weak or zero-point magnetic field without taking kinetic effects into account (cold plasma), a typical instability growth rate is an almost continuously increasing function of the transverse wave number  $k_{\perp}$ ,

$$\Gamma = \frac{\sqrt{3}}{2^{4/3}} \omega_{pe} \left( \frac{n_b}{n\gamma} \right)^{1/3} \left( \frac{k_{\parallel}^2}{k^2 \gamma^2} + \frac{k_{\perp}^2}{k^2} \right)^{1/3}, \quad (5)$$

where  $\Gamma$  is the growth rate,  $n_b$  is the beam density,  $n$  is the plasma density,  $\omega_{pe}$  is the fundamental electron frequency, and  $\gamma = 1/(1 - v_b^2/c^2)$  is the Lorentz factor for the beam velocity  $v_b$ . Growth in the beam temperature spreads, as well as increase in the magnetic field, leads to the suppression of the oblique instabilities.<sup>47</sup> Despite the fact that the linear framework is a significant simplification of the processes involved in the beam–plasma instability, it correctly predicts the spectrum of excited waves, even in simulations of realistic beam injection into plasma.<sup>55</sup>

In this paper, we consider beams with velocities  $v_b = 0.9c$  and  $v_b = 0.7c$ . Table I shows the parameters of the selected regimes, as well as the characteristics of the most unstable plasma beam modes: the excitation frequency  $\omega_b$ , the wavenumbers  $\mathbf{k} = (k_{\parallel}, k_{\perp}, 0)$ , and the growth rate value  $\Gamma$ . The first regime ( $v_b = 0.9c$ ) we will further call relativistic. The second one with  $v_b = 0.7c$ —sub-relativistic. Both beams have a Maxwellian energy spread

$$f_b(\mathbf{p}) \propto \exp\left(-\frac{(\mathbf{p} - \mathbf{p}_0)^2}{2\Delta p_b^2}\right),$$

and the temperature is defined as  $T_b = \Delta p_b^2/(2m_e)$ . At first, using the DispLib<sup>48</sup> library, we have calculated the unstable spectrum for the relativistic beam. It was found that the most unstable mode has the transverse wavenumber  $k_{\perp}^{max} = 2\omega_p/c$ . For the sub-relativistic beam, we decided to find a parameter when most unstable plasma wave also has transverse wavenumber  $k_{\perp}^{max} = 2\omega_p/c$ . Using of the same  $k_{\perp}^{max}$  for all regimes allows us to use the same transverse sizes of the simulation boxes. However, a lower energy of the beam leads to a lower level of transverse instability due to the reduction of relativistic mass anisotropy. In order to compensate this, we have to increase the relative density of the beam  $n_b/n_0$  and decrease its temperature, since the velocity spread mainly suppresses transverse unstable modes.<sup>47</sup> The resulting growth rate is higher than in the case of relativistic beam. This means that the relaxation length of such a beam will be smaller. One can also expect a larger amplitude of excited plasma oscillations in this case. In both modes, the background plasma temperature was  $T_p = 50$  eV. This temperature has no significant effect on the growth rate of the instability of such beams but is necessary for the stability of the numerical schemes in subsequent simulations. Also, the whole system is immersed in an external magnetic field  $\mathbf{B} = (B_0, 0, 0)$  such that  $\Omega_e = 0.1\omega_p$ , where  $\Omega_e = |e|B_0/m_e c$  is the cyclotron frequency of electrons.

**TABLE I.** Parameters of the beam–plasma system.

$v_b/c$	$n_b/n_0$	$T_b$ (keV)	$\Gamma/\omega_{p0}$	$\omega_b/\omega_{p0}$	$k_{\perp}^{max}, \omega_{p0}/c$	$k_{\parallel}^{max}, \omega_{p0}/c$
0.9	0.01	1	0.09	0.94	2	1.14
0.7	0.03	0.75	0.154	0.87	2	1.46

Furthermore, we will operate with dimensionless values. Plasma and beam particle densities will be calculated in units of  $n_0$ ; all frequencies in  $\omega_{p0} = \sqrt{4\pi n_0 e^2 / m_e}$ ; wave numbers in  $\omega_{p0}/c$ ; lengths in  $c/\omega_{p0}$ ; time in  $\omega_{p0}^{-1}$ ; electromagnetic fields measured in units of  $m_e c \omega_{p0}/c$ ; and particle speeds in the speed of light  $c$ . The conversion factors from dimensionless to dimensional units for various densities are available in the [Appendix](#).

[Figures 3 and 4](#) show the results of calculation of the growth rate for relativistic and sub-relativistic beams, respectively. For comparison, the line of maximum growth rate in the fluid approximation is also shown. Orange color marks the region of spectrum, where oscillations in the case of counter beams can participate in three-wave process of two Langmuir waves coupling into electromagnetic one with frequency equal to the doubled plasma frequency. It has been shown<sup>35</sup> that if the most unstable modes lie in this region, then, already at the linear stage of the beam–plasma instability, a highly efficient generation of electromagnetic radiation is possible. However, even a relatively small change of the system parameters accompanied by the violation of such localization of the maximum growth rate leads to a significant decrease in the emission level. Therefore, for the parameters chosen in this paper, we can be sure that not a three-wave process will determine the emission process of EM waves in the system.

#### IV. SIMULATION SETUP

For numerical simulations, we use our own 2D3V Cartesian parallel PIC code implemented for Nvidia GPGPU.<sup>49</sup> It is based on standard computational schemes: the Yee<sup>50</sup> solver of Maxwell equations for EM fields, the Boris<sup>51</sup> scheme for solving the equation of motion for collisionless macro-particles with a parabolic form factor, and the charge-conserving Esirkepov<sup>52</sup> scheme for calculations of currents. In all calculations, the spatial step of the computational grid was  $\Delta x = \Delta y = \pi/80 \approx 0.04$ , and the time step was  $\Delta t = 0.5\Delta x$ .

[Figure 5](#) shows a schematic of the computational region. Open boundary conditions<sup>36</sup> are used at its ends. They allow us to simulate the continuous injection of electron beams by self-consistent maintaining the compensating plasma current arising from the electron beam propagation. At the center of the computational domain a plasma column with a width of 720 cells ( $\approx 28.3c/\omega_{p0}$ ) is located, the plasma length  $L$  will be varied for different regimes. The continuously injected counter-streaming beams will have the same width  $\sigma$ , which we will

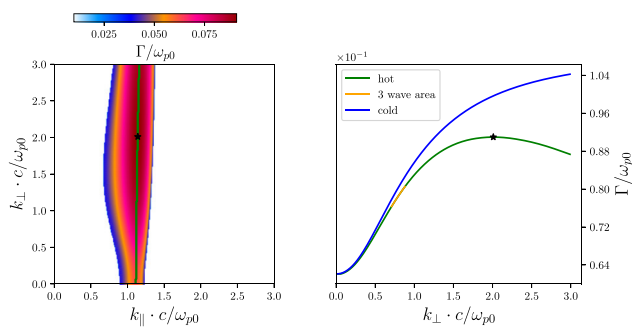


**FIG. 3.** Left: The growth rate map for the beam–plasma instability  $\Gamma(k_{||}, k_{\perp})$  for the beam with  $v_b = 0.9c$ . The green line  $k_{\perp} = k_{\perp}(k_{||})$  marks the local maximal growth rate. Right:  $\Gamma(k_{\perp})$  is on the line of the maximum (orange line indicates the region of the three-wave interaction). Blue line corresponds to the case of cold beam and plasma.

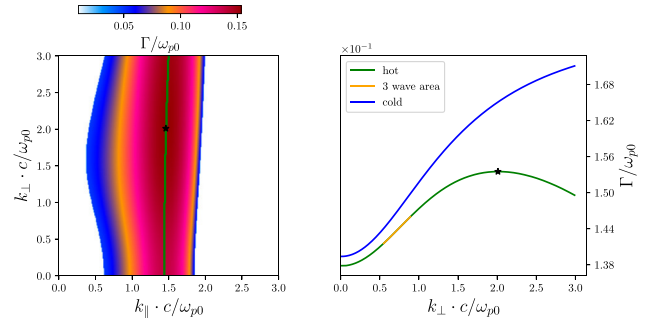


**FIG. 4.** Same as on the [Fig. 3](#), but for the beam with  $v_b = 0.7c$ .

vary in calculations from 3 to 9 transverse wavelengths  $\lambda_{\perp} = 2\pi/k_{\perp}^{max} = \pi$ . In [Fig. 5](#), the density of one relativistic beam at the moment of time shortly after it reaches the opposite boundary is shown. The transverse structure of the density perturbation arising due to the oblique instability is clearly seen. The injected beam current grows smoothly from zero to a given value in time  $50 \omega_{p0}^{-1}$  to avoid creating a seed to excite purely longitudinal oscillations by a sharp beam front.<sup>53</sup> The plasma is surrounded by vacuum and EM absorbing (damping) layers are located at the boundary. In this layer, the electromagnetic field values at each time step are multiplied by a coefficient  $k < 1$ , which decreases quadratically as a wave propagates deep into the layer. A full description of the implementation of open boundary conditions and absorbing layers is available in [Ref. 36](#). We will not consider the dynamics of plasma ions in this study, as it will interfere with a pure consideration of the process of interest.

#### V. SIMULATION RESULTS

Let us first consider the emission process in a system of counter-streaming relativistic beams.

##### A. Relativistic regime

Before proceeding to counter-beam simulations, two important issues have to be resolved. First, it is necessary to determine a sufficient

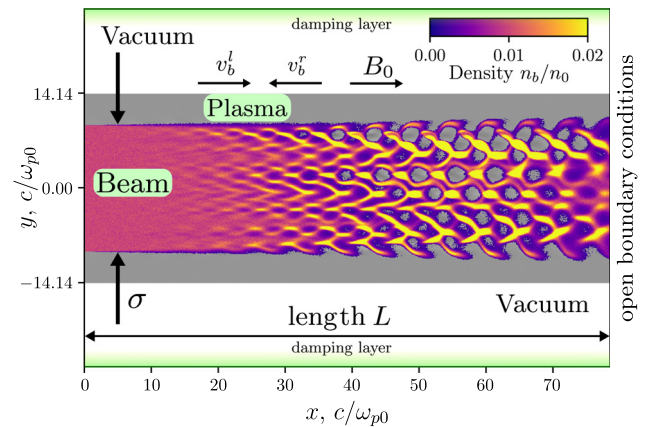


**FIG. 5.** Schematic of the computational region. The region occupied by background plasma is shown in gray.

number of macro-particles in a cell for the PIC simulation. For the most intense emission, the beams should build up the most intense plasma waves at the same place, so the longitudinal size  $L$  of the computational region should be approximately equal to twice the relaxation length of a single beam. So, second, we should find at what distance from the beam injection site there is a region of beam relaxation. Both questions can be answered by simulating single-beam injection.

### 1. Single beam

Since, in considering the relaxation process, we are not interested in emission processes, it is possible to simplify the computational domain by removing vacuum gaps, imposing periodic boundary conditions in transverse direction and reducing the thickness of the beam–plasma system to a few  $\lambda_{\perp}$ . This makes it possible to reduce the computational resource requirements and simplifies the study of the convergence of calculations on the number of particles per cell (ppc). In these calculations, we will be interested in two quantities. The first is the beam instability growth rate, which is calculated from the simulation results as follows:

$$\Gamma^{\text{PIC}}(t) = \frac{H'(t)}{2H(t)},$$

where  $H(t)$  is the energy of the electric field in the whole area.

The second quantity is the positioning of the beam relaxation region (the region of the most intense excitation of plasma oscillations). Since we have to take into account that the beam instability is oblique, we will trace the location and amplitude of the quantity  $E_0$ ,<sup>35</sup> which is calculated as the amplitude of plasma oscillations averaged over the length of plasma oscillations  $2l = 2\pi c/\omega_p$  in the longitudinal direction and integrated over the plasma thickness  $L_y$ ,

$$E_0(x, t) = \int_0^{L_y} dy \left[ \frac{\omega_p}{c\pi} \int_{-l}^l dx' E_x^2(x + x', y, t) \right]^{1/2}. \quad (6)$$

After calculation of  $E_0(x, t)$  at each diagnostic time step, the value of the amplitude maximum and its longitudinal position are determined.

Single-beam relaxation in plasma was simulated at system transverse sizes  $1\lambda_{\perp}$ ,  $2\lambda_{\perp}$ , and  $3\lambda_{\perp}$  (results were identical) for number of particles of each kind in a cell 100, 256, 400, and 900. Figure 6 shows the results. It can be seen that as the number of particles increases, there is no convergence to a single value. The observed differences seem to be caused by the dependence of the beam relaxation scenario on a particular implementation of the macro-particle distribution function, which is natural for PIC calculations of the beam–plasma interaction.<sup>35</sup> During the evolution of the beam instability, the relaxation region shifts. In the absence of ion dynamics, there is an initial excitation at some distance from the beam–plasma injection region followed by a shift toward the injector. Therefore, it can be expected that the most intense emission generation will be at the moment of crossing the relaxation regions of each beam, and then, a decrease in the emission level will be observed. At the same time, secondary maxima are possible on the time dependence of the emission level, caused by more complex dynamics of the interaction of counter beams in the plasma. The absolute value of the instability growth rate in the beam injection

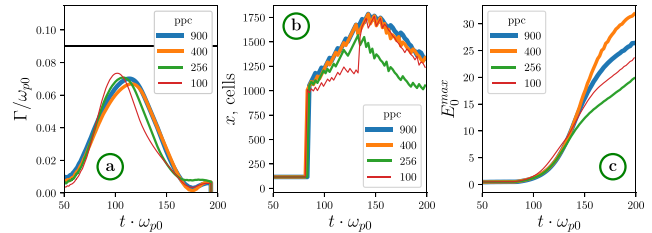


**FIG. 6.** Simulation of a single “relativistic” beam injection into plasma. The thickness of the system is  $3\pi$ . In transverse direction, periodic boundary conditions are realized. (a) Dependence of the instability growth rate  $\Gamma$  on time. Black horizontal line indicates a prediction of linear theory. (b) Dependence of the longitudinal coordinate of the maximum value of  $E_0(x, t)$ . (c) Dependence of the magnitude of the maximum  $E_0(x, t)$ .

simulations turned out to be somewhat smaller than theoretical predictions for an infinite beam–plasma system. Since 100 ppc allows us, with the available computational power, to investigate a larger range of thicknesses of the beam–plasma system, further calculations will be carried out with this number of ppc. Based on the dependence of  $E_0$  on the coordinate, we have chosen two lengths:  $L = 2 \times 1750\Delta x \approx 137.5 c/\omega_{p0}$  (long) and  $L = 2 \times 1000\Delta x \approx 78.5 c/\omega_{p0}$  (short).

Let us note that this is an approximate method of determining the optimal system size for radiation generation. Obviously, in a system with two beams, their relaxation follows a slightly different scenario from the one-beam case. The higher the relative density  $n_b$  of the beams and the further the two-beam instability process is from the linear regime, the stronger this difference will be. Therefore, if the goal is to maximize the level of EM emission, multiple simulations of different distances between the beam injection sites are required.

### 2. Counter-streaming beams

Figure 7 shows simulation results for the injection of counter-streaming relativistic beams with transverse size  $\sigma = 7\pi$  into a short plasma. Intense transverse emission can be seen from the region where the relaxation regions of each beams intersect. One can estimate their location by looking at the phase portrait  $f(v_{\parallel}, x)$  [Fig. 7(d)]. Figure 7(b) also shows the presence in the system of a small emission at a higher frequency. The radiation spectrum as a function of the longitudinal coordinate for each beam thickness is analyzed in detail in Fig. 8. It can be seen that there is no significant difference for each case. Apart from the main radiation near the second harmonic of the plasma frequency

$$(\omega_b, k_{\parallel}) + (\omega_b, -k_{\parallel}) \rightarrow (2\omega_b, 0), \quad (7)$$

there is also a small amount of radiation near the third and fourth harmonics, arising from the processes

$$(\omega_b, \mp k_{\parallel}) + (2\omega_b, \pm 2k_{\parallel}) \rightarrow (3\omega_b, \pm k_{\parallel}), \quad (8)$$

$$(2\omega_b, \pm 2k_{\parallel}) + (2\omega_b, 0) \rightarrow (4\omega_b, \pm 2k_{\parallel}). \quad (9)$$

These processes are essentially nonlinear and may be relevant for beams with high relative density that excite plasma oscillations of large amplitude.<sup>37</sup>

Figure 9 shows the beam-to-radiation power conversion efficiency. It can be seen that it reaches a value of a few percent and has

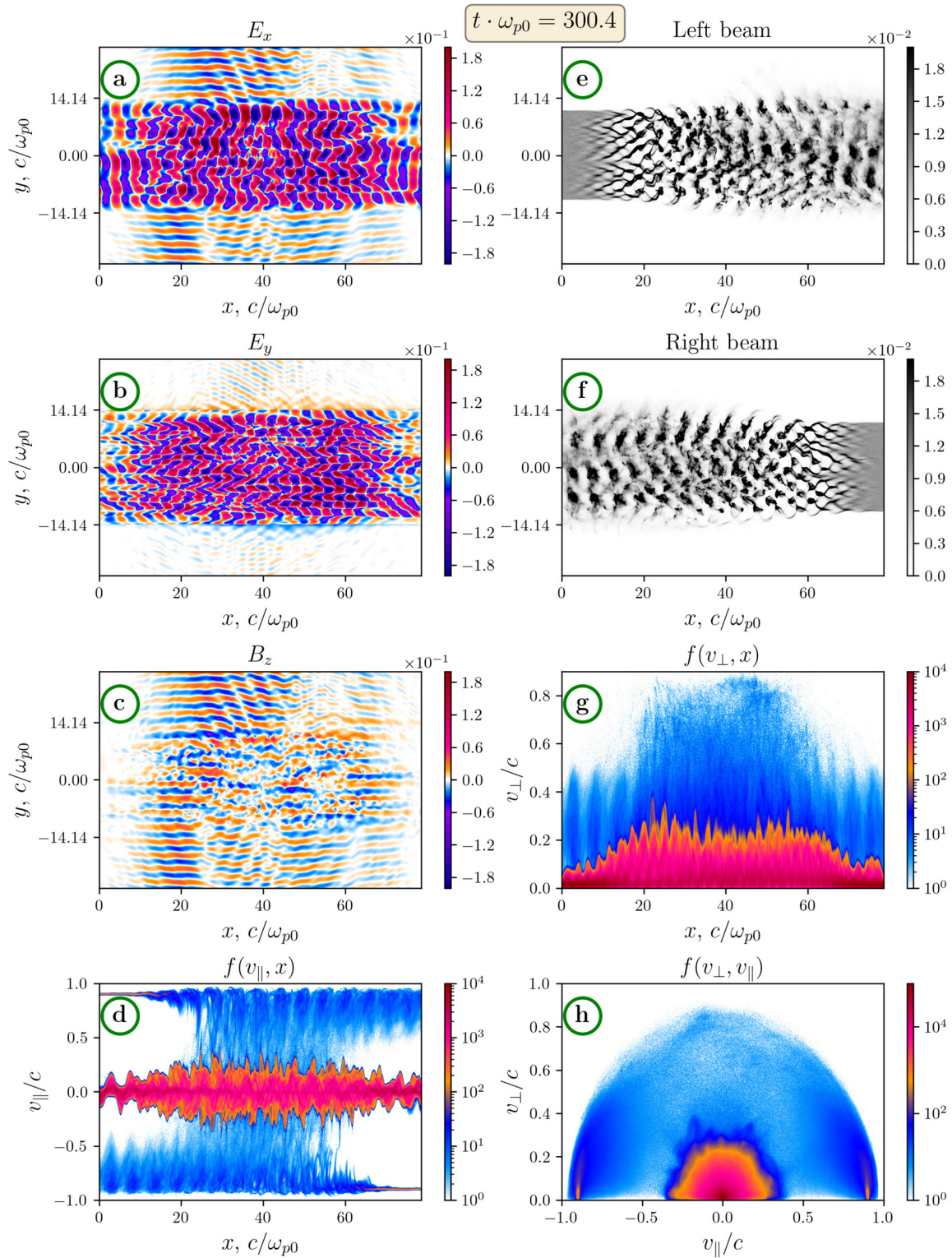


**FIG. 7.** Simulation results for relativistic counter-streaming beams. (a)–(c) components of electromagnetic fields. (e) and (f) beam density. (d), (g), and (h) plasma and beam electron velocity distribution functions. Beam thickness is  $\sigma = 7\pi$ , time moment:  $t \cdot \omega_{p0} \approx 300$ .

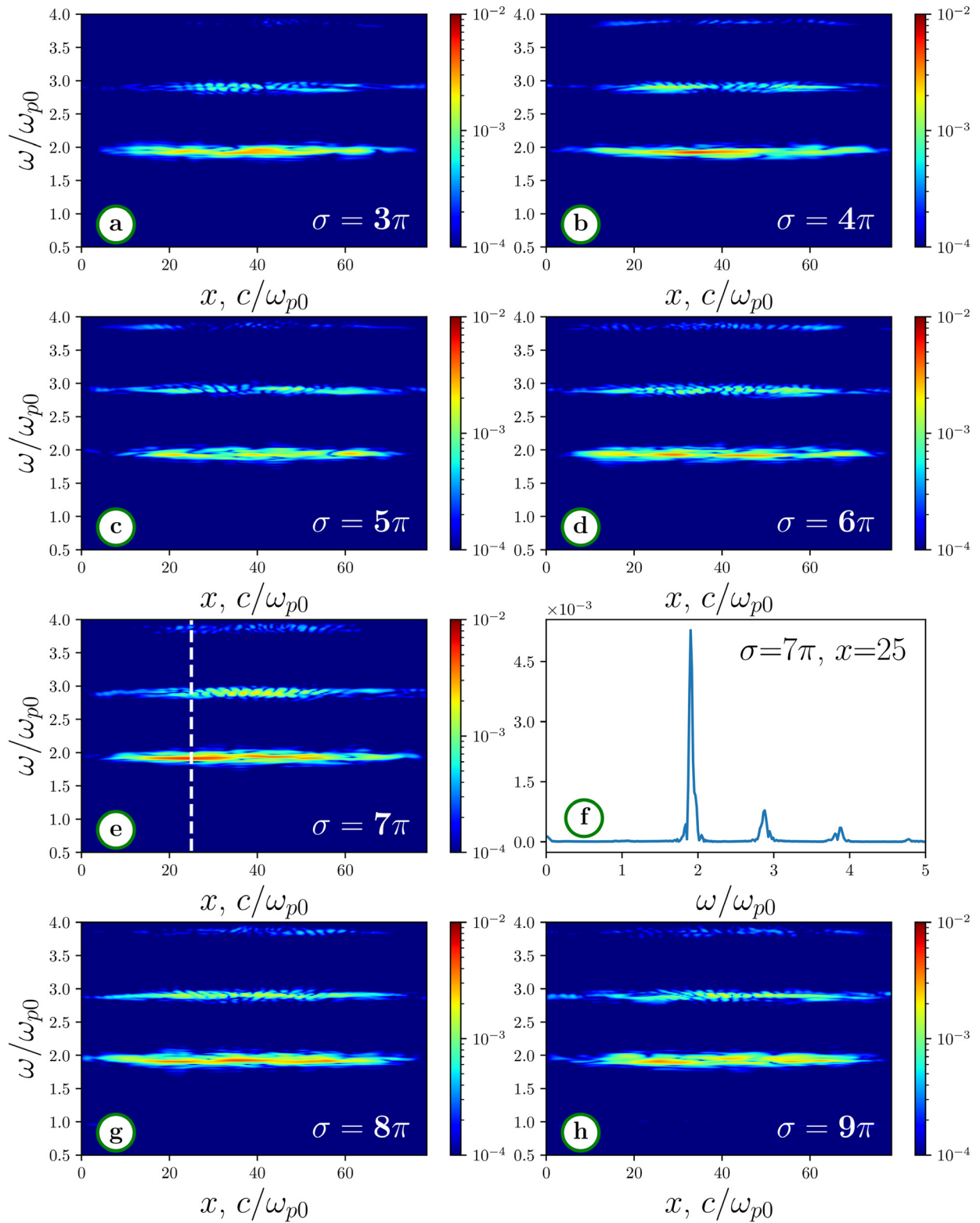
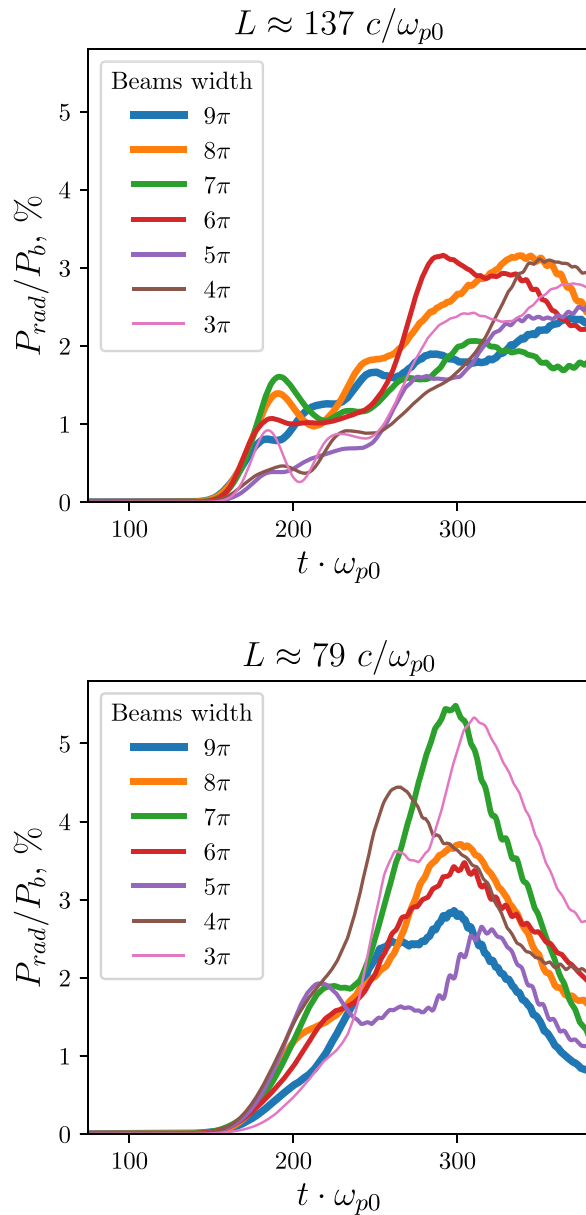


FIG. 8. Fourier spectrum of emission as a function of coordinate  $x$  for all  $\sigma$  in the case of counter-streaming relativistic beams. (f) Spectrum in  $x = 25c/\omega_{p0}$  for  $\sigma = 7\pi$ .

24 April 2024 04:38:02



**FIG. 9.** Efficiency of beam-to-radiation power conversion as a function of time for relativistic counter-streaming beams. Top: long system, bottom: short system. The plots are shown for all considered beam thicknesses.

no obvious dependence on thickness of the injected beams. However, in the case of *short* plasma, the radiation process is more efficient. One possible reason for this is that the emission process begins at the initial stage of instability, which is closer to linear. At this stage, there is a more distinct transverse structure of the excited waves. At large plasma lengths, the emission is generated from regions distant from the place of the development of the linear instability. Reaching them, the beams have a prehistory of interaction with the developed fields in the plasma and the oscillations excited by them have a transverse structure, which is less suitable for the generation of radiation.

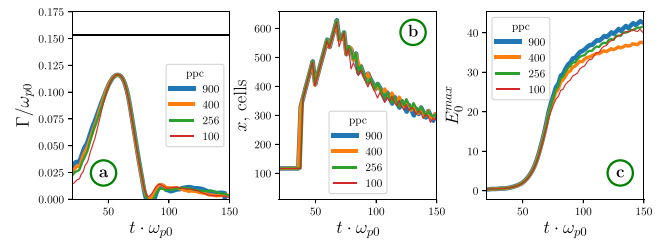


**FIG. 10.** Same as on Fig. 6, but for sub-relativistic beam.

## B. Sub-relativistic regime

Let us show that emission generation by the discussed mechanism for sub-relativistic beams is realized similarly to relativistic beams. As in Sec. V A 1, we first will investigate the convergence on the number of particles per cell, and also, we will estimate the relaxation length of a single beam by simulating a beam–plasma system with periodic boundary conditions in transverse direction and small thickness.

### 1. Single beam

Figure 10 shows the time dependence of the instability growth rate  $\Gamma(t)$  obtained in numerical simulations of single-beam injection into plasma with different ppc, as well as the localization and magnitude of the maximum  $E_0(x, t)$ . As in the case of the relativistic beam, no fundamental difference in the results has been observed for beam–plasma systems of different thicknesses ( $1\lambda_{\perp}$ ,  $2\lambda_{\perp}$ , and  $3\lambda_{\perp}$ ). Similarly to the previous regime, the maximum value of the growth rate is slightly lower than predicted by the linear theory. However, for this case, there is in fact a complete coincidence of the obtained dependencies for different ppc. From this, it is possible to conclude that for the chosen beam parameters, the development of instability is actually in hydrodynamic regime and less sensitive to details of reconstruction of distribution function by macro-particles.

For the considered sub-relativistic beam, the relaxation length is shorter than for the relativistic beam. The development of instability occurs earlier because of the larger growth rate. On the basis of obtained results, the beam–plasma system length for calculations with counter beams has been chosen equal to  $L = 2 \times 450\Delta x \approx 35.3 c/\omega_{p0}$ .

### 2. Counter-streaming beams

Similarly, as for the relativistic regime, we investigate the dependence of the radiation parameters on the transverse size of the injected beams. Figure 11 shows simulation results for beam widths  $\sigma = 6\lambda_{\perp}$ .

Figure 12 shows the histories of the radiation efficiency for different beam thicknesses. The result presented in the left figure looks as if some explicit dependence on the beam thicknesses takes place. To check this, we have carried out three simulations with  $\sigma = 6\lambda_{\perp}$  beams (right figure) and different actual realizations of the macro-particle distribution. It can be seen from the results that the observed differences in the radiation efficiency are related to these realizations and there is no clear dependence on the thickness of the beams. The maximum efficiency achieved is somewhat lower than in the relativistic mode. There can be different reasons for this, for example, smaller length of emitting region or more “flat form” of excited plasma oscillations, caused by the development of more intensive instability.

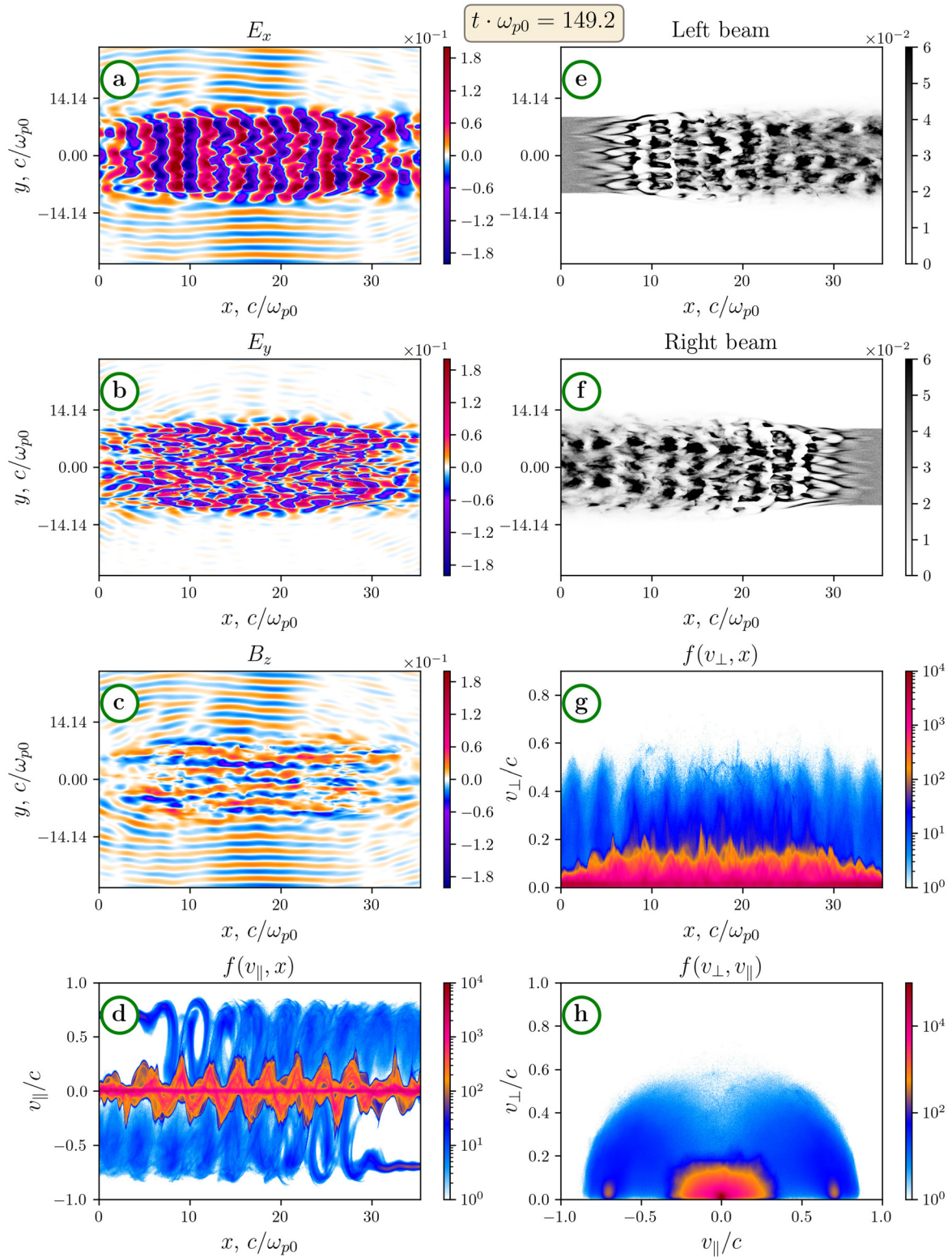
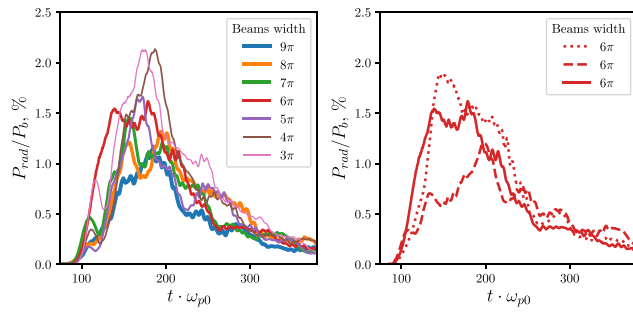


FIG. 11. Same as on Fig. 8. Sub-relativistic beams with thickness  $\sigma = 6\pi$ . Time moment  $t \cdot \omega_{p0} \approx 150$ .



**FIG. 12.** Efficiency of beam-to-radiation power conversion as a function of time for sub-relativistic counter-streaming beams. Left: all beam thicknesses except  $\sigma = 6\pi$ , right: three calculations with  $\sigma = 6\pi$ .

Figure 13 shows the emission spectrum over the whole computation time for beams with  $\sigma = 6\lambda_{\perp}$ . In this case, a slightly broader radiation is observed, which is also caused by the development of a more intense instability changing the parameters of the beam-plasma system and decreasing the emission duration.

### C. Beams with different velocities

Let us consider how the emission mechanism discussed would work in the case of different colliding beams. For this purpose, we carried out three simulations with identical initial macro-parameters in which the left beam was sub-relativistic and the right one was relativistic. The beam sizes  $\sigma = 6\lambda_{\perp}$  were equal, and the longitudinal length of the system was  $L = 1500\Delta x \approx 59 c/\omega_{p0}$ . The results obtained for run 1 are shown in Fig. 14. As in the previous regimes, the emission efficiency (Fig. 15) is a percentage of the beam power for all runs. The spectrum (Fig. 16) is dominated by radiation near the second harmonic of the plasma frequency, as expected.

Also, let us note the significant change in the phase portrait of the beams seen in Fig. 14(d) caused by interaction with large-amplitude plasma oscillations. In this case, we cannot any more consider that the oscillations are excited by beams with a velocity  $v_b$  given at the time of injection. Instead, it is more correct to consider some effective beam velocity. Let us define this velocity  $v_b^{eff}$  as follows. Assume that the

injected electron beam after propagating through a region with previously excited plasma oscillations acquires a complex distribution function determined by both the energy loss and heating of the beam and the process of trapping of the beam in the plasma wave. At the considered location, the beam undergoes the two-stream instability and excites plasma waves with a frequency  $\omega'_b \approx \omega_{p0}$  and a wavenumber  $k'_{\parallel}$ . By the effective beam velocity, we mean the velocity of the monoenergetic beam at which  $k'_{\parallel} = \omega_{p0}/v_b^{eff}$ . Due to the change in velocity, the wavenumber of plasma oscillations excited also changes. However, in the case of symmetric counter beams, this does not change the angle of radiation generation due to the identical change of  $v_b^{eff}$  for both beams.

Let us estimate the emission angle predicted from the theory. The longitudinal wavenumber of the radiation-generating perturbation is calculated from the wavenumbers of the oscillations excited by each beam (Table I)

$$k_{\parallel} = k_{\parallel}^{(1)} - k_{\parallel}^{(2)}$$

$$k_{\parallel} = 1.46 - 1.14 = 0.32.$$

The oscillation frequency can be obtained from the sum of the theoretical frequencies  $\omega_r = 0.94 + 0.87 = 1.81$ . Then, the transverse wavenumber of radiation should be  $k_{\perp} = \sqrt{\omega_r^2 - k_{\parallel}^2} = 1.78$  and the angle of emission 4:  $\alpha \approx 10^\circ$ . Radiation at this angle is indeed observed, but only at the very beginning of the instability development process [Fig. 17(a)]. Then, the distribution of the freshly injected sub-relativistic beam changes dramatically under the action of previously excited plasma oscillations [Fig. 14(d)]. Since, in contrast to the case of symmetric beam injection (Sec. VB2), in this case the second beam (relativistic) does not experience a symmetric change in effective velocity, a significant change in the emission angle is observed [Fig. 17(b)]. The further away the sub-relativistic beam is from the injection site, the lower its effective velocity and the larger the emission angle. Near the region of relativistic beam injection one observes an emission angle of about 50 deg. Since at this place, the effective speed of the right beam has not yet had time to change essentially, from the angle of radiation, we can estimate the effective speed of the sub-relativistic beam, which was  $v_{eff} \approx 0.3c$ .

Note that this does not mean that the total beam energy has decreased by nearly 90% after passing through the plasma, dropping to a value corresponding to the velocity  $v \approx 0.3c$ . Based on measurements of the beam energy flux at the entrance and exit of the system, its energy loss can be estimated at  $\approx 33\%$ . Some of this energy was lost to radiation and the other part to heating of plasma and excitation of non-emitting plasma oscillations.

### VI. DISCUSSION AND CONCLUSION

Let us briefly summarize the main results of this paper:

1. The emission mechanism during the interaction of counter-propagating plasma waves with different transverse structure is effectively realized for plasmas with two counter-streaming electron beams in the regime of oblique small-scale instability dominance.
2. These regimes can be predicted by the exact linear theory of the beam-plasma instability without full-scale PIC simulations.
3. On the scales considered in this article, there is no dependence of the generation efficiency on the thickness of electron beams.

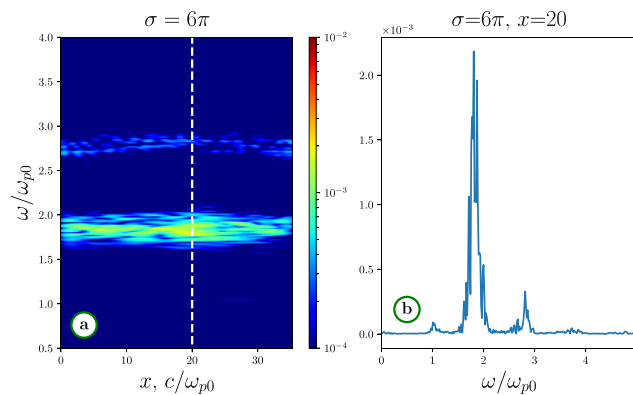


**FIG. 13.** Fourier spectrum of emission for sub-relativistic counter-streaming beams with  $\sigma = 6\pi$ .

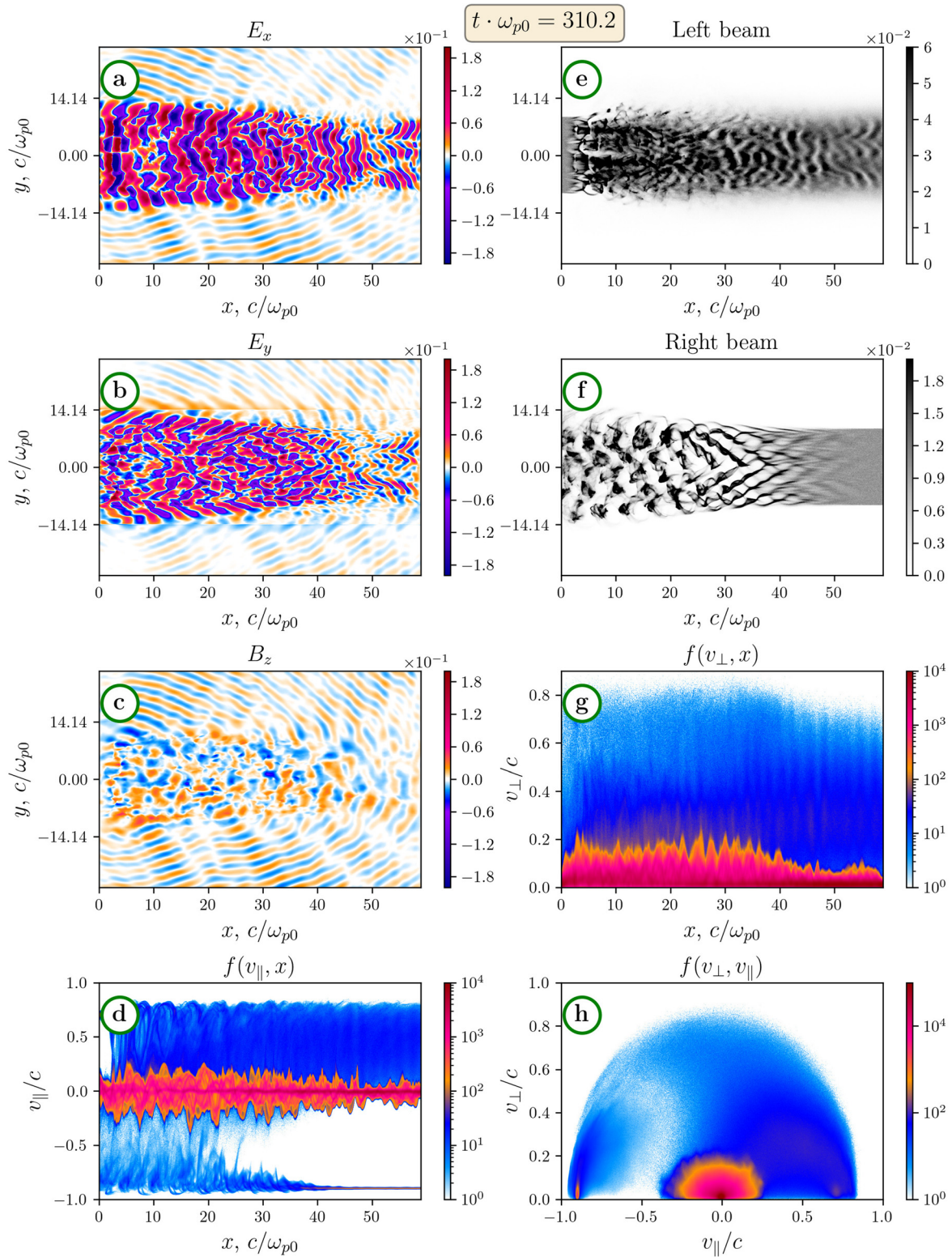
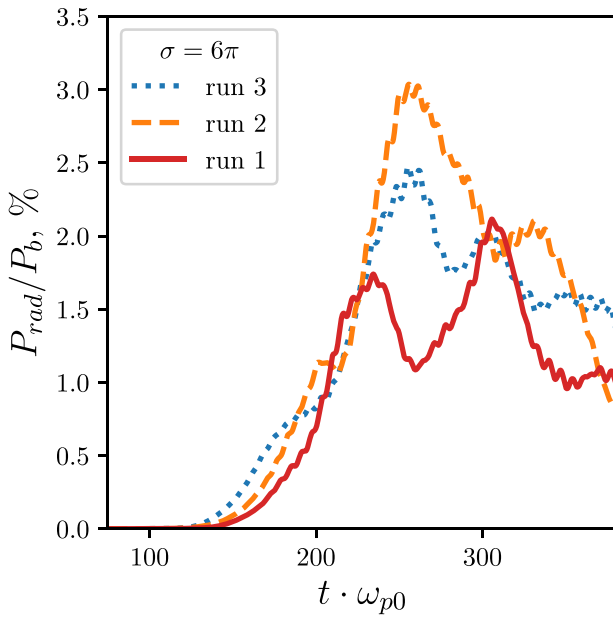


FIG. 14. Same as on Fig. 8. Relativistic and sub-relativistic beams with thickness  $\sigma = 6\pi$ . Time moment  $t \cdot \omega_{p0} \approx 310$  for run 1.

24 April 2024 04:38:02



**FIG. 15.** Efficiency of beam-to-radiation power conversion as a function of time for counter-streaming relativistic and sub-relativistic beams.

Also, the spectrum of radiation is the same, since the generation takes place at harmonics of plasma frequency starting from the second one. The surrounding plasma is transparent for such radiation.

4. Beam-to-radiation power conversion efficiency for all modes considered is at the level of a few percent, which is a sufficiently high value for beam-plasma systems.

In the work,<sup>35</sup> emission at the second harmonic of plasma frequency was also considered in the system with counter-streaming beams in plasma, but due to the three-wave merging process of plasma waves into electromagnetic ones. It has been demonstrated that achieving radiation generation with an efficiency of a few percent of the beam power requires precise parameter selection for the system. In

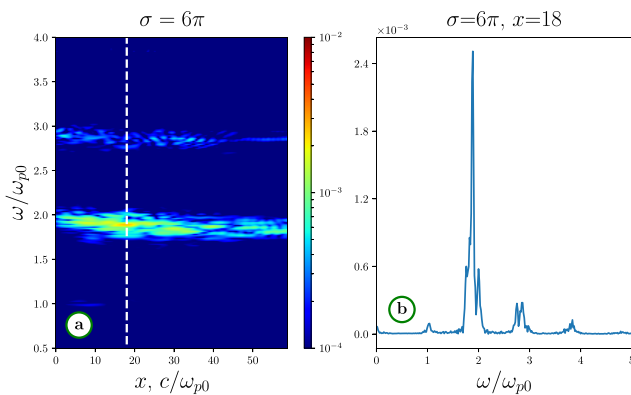


**FIG. 16.** Emission spectrum for counter-streaming relativistic and sub-relativistic beams (run 1).

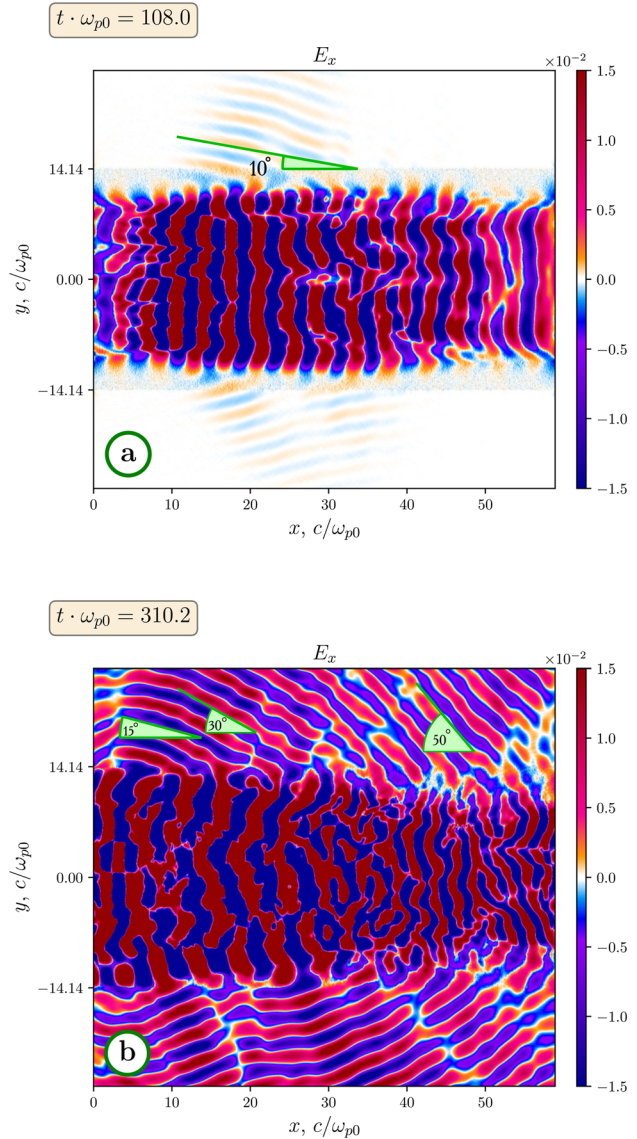


**FIG. 17.** The field  $E_x$  for counter-streaming relativistic and sub-relativistic beams. (a) The initial moment of development of the instability and (b) the later one are shown. Angles of radiation with respect to the system's axis are marked in green.

this regime, the most unstable modes of plasma oscillations lie exactly in a certain region of the spectrum for which the necessary three-wave process is allowed. Even an insignificant change of parameters of the system, which leads to leaving this region, means a decrease in efficiency of radiation generation in times. Thus, this mechanism appears to be extremely sensitive to the parameters of the system and even a small change of them can interrupt the generation of radiation. In contrast to it, the mechanism considered in this work does not require exact selection of system parameters and should work with similar efficiency in a wide range of parameters, at which oblique modes of plasma oscillations dominate. The specific impact of density gradients

(regular and random) on electron beam relaxation in plasma is still the subject of intense research.<sup>30,54–56</sup> In the case of regular gradients, we can expect that this emission mechanism will still work, while gradients are not large enough to stabilize the beam–plasma instability. Same is also for random gradients. However, in former case, one can expect radiation near the fundamental frequency and its harmonics due to scattering of plasma waves on small-scale density perturbations. Similar density perturbations can arise in self-consistently manner during the relaxation process due to modulation instability.<sup>29</sup> They can cause localized disruption of the beam–plasma instability. In this case, each beam begins to build up plasma waves in more distant regions, and the overlap region decreases. The main emission near  $2\omega_{pe}$  will decrease. However, after some time, the density perturbations can relax and favorable conditions for the new buildup cycle of the beam–plasma instability will be restored.<sup>29</sup>

In this work, we consider the head-on collision of electron beams propagating along an external magnetic field. The presence of a small angle between the propagation axes of the beams should slightly alter the relaxation scenario and induce gyro emission processes. However, if the beams build up the necessary plasma waves,  $2\omega_p$  emission should also occur. This radiation process for the oblique collision of two thin electron beams without an external magnetic field was investigated in the work.<sup>38</sup>

Let us discuss what practical recommendations can be made on the basis of these results. There are two areas, for which the considered mechanism of radiation generation may be relevant. The first one is generation of powerful, frequency-tunable narrowband radiation in laboratory plasma. Using the exact linear theory, it is possible to choose parameters of the beam–plasma system and, with the help of PIC simulation, to estimate the efficiency of generation and the beam relaxation length, which is necessary for the design of radiation sources.

The second one is the sources of non-thermal radio emission in astrophysical systems and especially in solar plasma. Systems with counter electron fluxes can arise at interaction of the curved front of shock waves with magnetic field lines or in the case of closely spaced regions of intense energy release due to magnetic reconnection. By estimating the parameters of the surrounding plasma, such as thermal and x-ray radiation, from measurements, and utilizing existing models of similar systems, one can incorporate these parameters into an exact linear algorithm. This algorithm calculates the growth rate of the beam–plasma instability and provides an estimate of the possibility of radiation generation by the discussed mechanism.

Of further interest in the research of this generation, mechanism is the question about dependence of radiation parameters on transverse length of excited oscillations. Study of regimes with smaller and larger energy beams is also relevant to this investigation, as well as consideration of the relaxation process in plasma with large- and small-scale density inhomogeneities and full-scale 3D3V PIC simulations.

**SUPPLEMENTARY MATERIAL**

See the supplementary material for the videos of the radiation generation process with counter plasma waves from Sec. II, as well as the videos of all electron beam simulations, are available in the supplementary material. In all those videos, we show: (a) longitudinal electric field  $E_x$ ; (b) electric field  $E_y$ ; (c) magnetic field  $B_z$ ; (d) the density  $n_b/n_0$  of the beam injected from the left side of the simulation box; (e) the density  $n_b/n_0$  of the oppositely injected beam (for runs with two beams); (f) the plasma electron density  $n_e/n_0$ ; the velocity distribution

functions of the plasma and beam electrons: (g)  $f(v_{\parallel}, x)$ , where  $v_{\parallel} \equiv v_x$ ; (h)  $f(v_{\perp}, x)$ , where  $v_{\perp} = \sqrt{v_x^2 + v_y^2}$ ; and (i)  $f(v_{\perp}, v_{\parallel})$ .

**ACKNOWLEDGMENTS**

The work was supported by the Ministry of Science and Higher Education of the Russian Federation and by the Foundation for the Advancement of Theoretical Physics and Mathematics “BASIS.” Simulations were performed using the computing resources of the Center for Scientific IT-services ICT SB RAS.

**AUTHOR DECLARATIONS**

**Conflict of Interest**

The authors have no conflicts to disclose.

**Author Contributions**

**Vladimir Vadimovich Annenkov:** Conceptualization (lead); Data curation (lead); Formal analysis (lead); Investigation (lead); Methodology (equal); Project administration (equal); Software (lead); Visualization (lead); Writing – original draft (lead). **Evgeniya Volchok:** Conceptualization (supporting); Methodology (supporting); Software (supporting); Writing – review & editing (equal). **Igor Timofeev:** Funding acquisition (lead); Methodology (equal); Project administration (equal); Writing – review & editing (equal).

**DATA AVAILABILITY**

The data that support the findings of this study are available within the supplementary material.

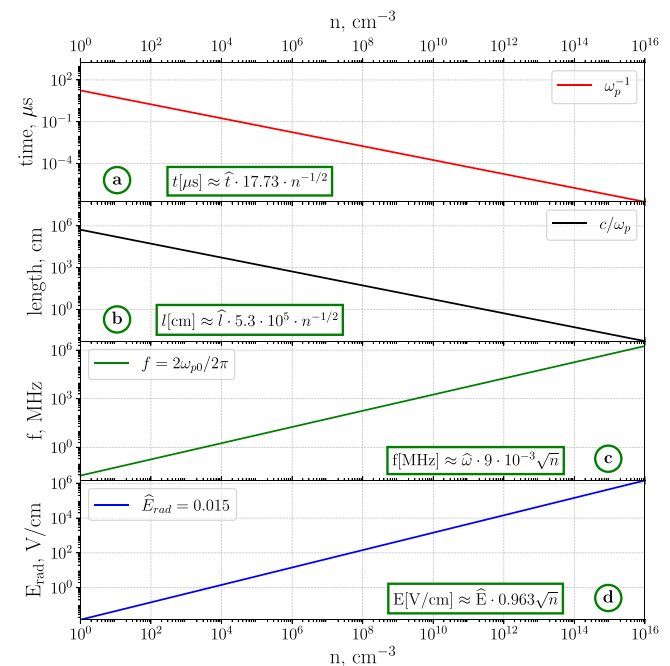


**FIG. 18.** Correspondence between dimensional and dimensionless quantities on a logarithmic scale. (a) The unit of time  $\omega_{p0}^{-1}$ . (b) The unit of length  $c/\omega_{p0}$ . (c) The linear frequency of radiation at the second harmonic of the plasma frequency. (d) The characteristic amplitude of the radiation electric field.

24 April 2024 04:38:02

## APPENDIX: DIMENSIONAL CONVERSION

The processes we study can take place in plasma systems with widely varying densities: from low-dense solar wind to high-dense plasma in laboratory devices. On Fig. 18, we show conversion of main dimensionless values (time, length, and emission frequency on  $2\omega_{pe}$ ), as well as the characteristic amplitude of the radiation electric field. In simulations, typical dimensionless amplitude of emission was observed between 0.01 and 0.02.

## REFERENCES

- <sup>1</sup>A. I. Akhiezer and Y. B. Fainberg, "On the interaction of charged particle beam with electron plasma," *Dokl. Akad. Nauk USSR* **69**, 555 (1949).
- <sup>2</sup>D. Bohm and E. P. Gross, "Theory of plasma oscillations. B. Excitation and damping of oscillations," *Phys. Rev.* **75**, 1864 (1949).
- <sup>3</sup>A. Burdakov, A. Azhannikov, V. Astrelin, A. Beklemishev, V. Burmasov, G. Derevyankin, V. Ivanenko, I. Ivanov, M. Ivantsivsky, I. Kandaurov, V. Konyukhov, I. Kotelnikov, V. Kovenya, T. Kozlinskaya, K. Kuklin, A. Kuznetsov, S. Kuznetsov, K. Lotov, I. Timofeev, A. Makarov, K. Mekler, V. Nikolaev, S. Popov, V. Postupaev, S. Polosatkin, A. Rovenskikh, A. Shoshin, I. Shvab, S. Sinitsky, Y. Sulyaev, V. Stepanov, Y. Trunov, L. Vyacheslavov, V. Zhukov, and E. Zubairov, "Plasma heating and confinement in GOL-3 multi mirror trap," *Fusion Sci. Technol.* **51**, 106–111 (2007).
- <sup>4</sup>A. V. Burdakov, A. V. Arzhannikov, V. S. Burmasov, I. A. Ivanov, M. V. Ivantsivsky, I. V. Kandaurov, S. A. Kuznetsov, V. V. Kurkuchekov, K. I. Mekler, S. V. Polosatkin, S. S. Popov, V. V. Postupaev, A. F. Rovenskikh, V. F. Sklyarov, M. K. A. Thumm, Y. A. Trunov, and L. N. Vyacheslavov, "Microwave generation during 100 keV electron beam relaxation in GOL-3," *Fusion Sci. Technol.* **63**, 286–288 (2013).
- <sup>5</sup>E. Soldatkina, E. Pinzhnin, O. Korobeynikova, V. Maximov, D. Yakovlev, A. Solomakhin, V. Savkin, K. Kolesnichenko, A. Ivanov, Y. Trunov, R. Voskoboynikov, G. Shulzhenko, V. Annenkov, E. Volchok, I. Timofeev, and P. Bagryansky, "Electron beam-plasma discharge in GDT mirror trap: Experiments on plasma start-up with electron gun," *Nucl. Fusion* **62**, 066034 (2022).
- <sup>6</sup>A. V. Arzhannikov, I. A. Ivanov, A. A. Kasatov, S. A. Kuznetsov, M. A. Makarov, K. I. Mekler, S. V. Polosatkin, S. S. Popov, A. F. Rovenskikh, D. A. Samstov, S. L. Sinitsky, V. D. Stepanov, V. V. Annenkov, and I. V. Timofeev, "Well-directed flux of megawatt sub-mm radiation generated by a relativistic electron beam in a magnetized plasma with strong density gradients," *Plasma Phys. Controlled Fusion* **62**, 045002 (2020).
- <sup>7</sup>Ashish, K. Gopal, S. Singh, and D. N. Gupta, "High-intensity laser pulse interaction with a counter propagating electron beam for terahertz field generation in magnetized plasmas," *Opt. Quantum Electron.* **55**, 605 (2023).
- <sup>8</sup>D. N. Gupta, M. C. Gurjar, and A. Jain, "Terahertz generation by a rotating relativistic electron beam in a magnetized plasma column," *J. Plasma Phys.* **89**, 905890410 (2023).
- <sup>9</sup>B. N. Breizman, P. Aleynikov, E. M. Hollmann, and M. Lehnen, "Physics of runaway electrons in tokamaks," *Nucl. Fusion* **59**, 083001 (2019).
- <sup>10</sup>M. Hoppe, I. Ekmark, E. Berger, and T. Fülöp, "Runaway electron generation during tokamak start-up," *J. Plasma Phys.* **88**, 905880317 (2022).
- <sup>11</sup>E. R. Sanchez, A. T. Powis, I. D. Kaganovich, R. Marshall, P. Porazik, J. Johnson, M. Greklek-McKeon, K. S. Amin, D. Shaw, and M. Nicolls, "Relativistic particle beams as a resource to solve outstanding problems in space physics," *Front. Astron. Space Sci.* **6**, 71 (2019).
- <sup>12</sup>Y. V. Khotyaintsev, D. B. Graham, C. Norgren, and A. Vaivads, "Collisionless magnetic reconnection and waves: Progress review," *Front. Astron. Space Sci.* **6**, 1–20 (2019).
- <sup>13</sup>M. Lazar, R. A. López, P. S. Moya, S. Poedts, and S. M. Shaaban, "The aperiodic firehose instability of counter-beaming electrons in space plasmas," *Astron. Astrophys.* **670**, A85 (2023).
- <sup>14</sup>S.-Y. Lee, P. H. Yoon, E. Lee, and W. Tu, "Simulation of plasma emission in magnetized plasmas," *Astrophys. J.* **924**, 36 (2022).
- <sup>15</sup>L. F. Ziebell, "Weakly turbulent plasma processes leading to plasma emission in the presence of a ring-beam electron population," *Astrophys. Space Sci.* **366**, 60 (2021).
- <sup>16</sup>D. I. Pontin and E. R. Priest, *Living Reviews in Solar Physics* (Springer International Publishing, 2022), Vol. 19.
- <sup>17</sup>A. Marcowith, A. Bret, A. Bykov, M. E. Dieckman, L. O. Drury, B. Lembège, M. Lemoine, G. Morlino, G. Murphy, G. Pelletier, I. Plotnikov, B. Reville, M. Riquelme, L. Sironi, and A. S. Novo, "The microphysics of collisionless shock waves," *Rep. Prog. Phys.* **79**, 046901 (2016).
- <sup>18</sup>R. V. Lovelace and R. N. Sudan, "Plasma heating by high-current relativistic electron beams," *Phys. Rev. Lett.* **27**, 1256–1259 (1971).
- <sup>19</sup>D. Cromwell, P. McQuillan, and J. C. Brown, "Beam-driven return current instability and anomalous plasma heating in solar flares," *Sol. Phys.* **115**, 289–312 (1988).
- <sup>20</sup>M. J. Aschwanden, "Particle acceleration and kinematics in solar flares: A synthesis of recent observations and theoretical concepts (invited review)," *Space Sci. Rev.* **101**, 1–227 (2002).
- <sup>21</sup>V. L. Ginzburg and V. V. Zheleznyakov, "On the possible mechanisms of sporadic solar radio emission (radiation in an isotropic plasma)," *Sov. Astron.* **2**, 653–668 (1958).
- <sup>22</sup>H. A. S. Reid and H. Ratcliffe, "A review of solar type III radio bursts," *Res. Astron. Astrophys.* **14**, 773–804 (2014).
- <sup>23</sup>M. Aschwanden, *Physics of the Solar Corona*, Springer Praxis Books, 2nd ed. (Springer, Berlin, Heidelberg, 2005).
- <sup>24</sup>I. V. Timofeev, V. V. Annenkov, and A. V. Arzhannikov, "Regimes of enhanced electromagnetic emission in beam-plasma interactions," *Phys. Plasmas* **22**, 113109 (2015).
- <sup>25</sup>V. V. Annenkov, E. P. Volchok, and I. V. Timofeev, "Generation of high-power electromagnetic radiation by a beam-driven plasma antenna," *Plasma Phys. Controlled Fusion* **58**, 045009 (2016).
- <sup>26</sup>V. V. Annenkov, E. A. Berendeev, E. P. Volchok, and I. V. Timofeev, "Second harmonic electromagnetic emission in a beam-driven plasma antenna," *Plasma Phys. Controlled Fusion* **61**, 055005 (2019).
- <sup>27</sup>V. Glinitskiy, I. Timofeev, and V. Annenkov, "Efficient generation of  $\omega_p$ -radiation in a beam-driven thick plasma with oblique density modulation," *J. Plasma Phys.* **15**, 905880309 (2022).
- <sup>28</sup>V. V. Annenkov, I. V. Timofeev, and E. P. Volchok, "Simulations of electromagnetic emissions produced in a thin plasma by a continuously injected electron beam," *Phys. Plasmas* **23**, 053101 (2016).
- <sup>29</sup>V. V. Annenkov, I. V. Timofeev, and E. P. Volchok, "Highly efficient electromagnetic emission during 100 keV electron beam relaxation in a thin magnetized plasma," *Phys. Plasmas* **26**, 063104 (2019).
- <sup>30</sup>V. Annenkov and E. Volchok, "Numerical simulations of a continuously injected relativistic electron beam relaxation into a plasma with large-scale density gradients," *Adv. Space Res.* **71**, 1948–1961 (2023).
- <sup>31</sup>U. Ganse, P. Kilian, R. Vainio, and F. Spanier, "Emission of type II radio bursts- single-beam versus two-beam scenario," *Sol. Phys.* **280**, 551–560 (2012).
- <sup>32</sup>P. Leung, J. Santoru, A. Y. Wong, and P. Y. Cheung, "Observation of electromagnetic radiation at  $2\omega_p$  generated by Beam-Plasma interactions," in *Physics of Auroral Arc Formation*, edited by J. R. Akasofu and S.-I. Kan (American Geophysical Union, Washington, 1981), pp. 387–392.
- <sup>33</sup>T. Intrator, N. Hershkowitz, and C. Chan, "Experimental observations of nonlinearly enhanced  $2\omega_{UH}$  electromagnetic radiation excited by steady-state colliding electron beams," *Phys. Fluids* **27**, 527 (1984).
- <sup>34</sup>R. W. Schumacher, J. Santoru, M. Rosenberg, and N. A. Krall, "Microwave/millimeter-wave generation in a counterstreaming-beam-plasma system," *J. Appl. Phys.* **74**, 3057–3060 (1993).
- <sup>35</sup>V. V. Annenkov, E. P. Volchok, and I. V. Timofeev, "Electromagnetic emission produced by three-wave interactions in a plasma with continuously injected counterstreaming electron beams," *Astrophys. J.* **904**, 88 (2020).
- <sup>36</sup>V. V. Annenkov, E. A. Berendeev, I. V. Timofeev, and E. P. Volchok, "High-power terahertz emission from a plasma penetrated by counterstreaming different-size electron beams," *Phys. Plasmas* **25**, 113110 (2018).
- <sup>37</sup>V. Annenkov, E. A. Berendeev, E. Volchok, and I. Timofeev, "Particle-in-cell simulations of high-power THz generator based on the collision of strongly focused relativistic electron beams in plasma," *Photonics* **8**, 172 (2021).
- <sup>38</sup>M. Kumar, T. Kang, H. S. Song, and M. S. Hur, "Particle-in-cell simulations of THz emission from plasma by oblique collision of two-electron beams," *Phys. Plasmas* **29**, 033102 (2022).

- <sup>39</sup>I. V. Timofeev, V. V. Annenkov, and E. P. Volchok, "Generation of high-field narrowband terahertz radiation by counterpropagating plasma wakefields," *Phys. Plasmas* **24**, 103106 (2017).
- <sup>40</sup>E. Volchok, V. Annenkov, and I. Timofeev, "Electromagnetic emission due to nonlinear interaction of laser wakefields colliding in plasma at an oblique angle," *Plasma Phys. Controlled Fusion* **63**, 045001 (2021).
- <sup>41</sup>V. V. Annenkov, I. V. Timofeev, E. A. Berendeev, and E. P. Volchok, "Powerful electromagnetic emission from a plasma with counterstreaming different-size electron beams," in 46th EPS Conference on Plasma Physics (EPS 2019) (European Physical Society, 2019).
- <sup>42</sup>I. V. Timofeev, "Two-dimensional simulations of nonlinear beam-plasma interaction in isotropic and magnetized plasmas," *Phys. Plasmas* **19**, 042108 (2012).
- <sup>43</sup>E. P. Volchok, V. V. Annenkov, E. A. Berendeev, and I. V. Timofeev, "Generation of narrow-band THz radiation by collision of laser wake waves with a small-scale transverse structure in a plasma," *Bull. Lebedev Phys. Inst.* **50**, 272–277 (2023).
- <sup>44</sup>E. A. Berendeev, I. V. Timofeev, E. P. Volchok, and V. V. Annenkov, "PIC simulations of high-power THz radiation produced by the collision of profiled plasma wakefields," *J. Phys.: Conf. Ser.* **2028**, 012008 (2021).
- <sup>45</sup>S. A. Bludman, K. M. Watson, and M. N. Rosenbluth, "Statistical mechanics of relativistic streams. II," *Phys. Fluids* **3**, 747–757 (1960).
- <sup>46</sup>B. N. Breizman, *Voprosy Teorii Plazmy*, edited by B. B. Kadomtsev (Energoatomizdat, 1987), Vol. 15, p. 60.
- <sup>47</sup>I. V. Timofeev and V. V. Annenkov, "Exact kinetic theory for the instability of an electron beam in a hot magnetized plasma," *Phys. Plasmas* **20**, 092123 (2013).
- <sup>48</sup>V. V. Annenkov, E. P. Volchok, and I. V. Timofeev, "Numerical code for calculating plasma waves dispersion in relativistic magnetized plasma," in 47th EPS Conference on Plasma Physics (EPS 2021) (European Physical Society, 2021), pp. 125–128.
- <sup>49</sup>E. Lindholm, J. Nickolls, S. Oberman, and J. Montrym, "NVIDIA Tesla: A unified graphics and computing architecture," *IEEE Micro* **28**, 39–55 (2008).
- <sup>50</sup>K. S. Yee, "Numerical solution of initial boundary value problems involving Maxwell's equations in isotropic media," *IEEE Trans. Antennas Propag.* **14**, 302–307 (1966).
- <sup>51</sup>J. P. Boris, "Relativistic plasma simulation-optimization of a hybrid code," in Proceeding of Fourth Conference on Numerical Simulations of Plasmas (Naval Research Laboratory, Washington DC, 1970), pp. 3–67.
- <sup>52</sup>T. Esirkepov, "Exact charge conservation scheme for particle-in-cell simulation with an arbitrary form-factor," *Comput. Phys. Commun.* **135**, 144–153 (2001).
- <sup>53</sup>E. P. Volchok, V. V. Annenkov, I. V. Timofeev, and E. A. Berendeev, "Efficient electromagnetic emission from plasma with continuously injected counterstreaming electron beams," in 46th EPS Conference on Plasma Physics (EPS 2019) (European Physical Society, 2019).
- <sup>54</sup>C. Krafft and P. Savoini, "Dynamics of two-dimensional type III electron beams in randomly inhomogeneous solar wind plasmas," *Astrophys. J.* **949**, 24 (2023).
- <sup>55</sup>P. V. Vatagin and I. V. Kudryavtsev, "Spatio-temporal dynamics of fast electrons and plasma turbulence in an inhomogeneous flare plasma," *Geomagn. Aeron.* **61**, 1135–1140, <https://doi.org/10.1134/S001679322108020X> (2021).
- <sup>56</sup>M. Shalaby, A. E. Broderick, P. Chang, C. Pfrommer, E. Puchwein, and A. Lamberts, "The growth of the longitudinal beam-plasma instability in the presence of an inhomogeneous background," *J. Plasma Phys.* **86**, 535860201 (2020).